A truly Lego®-like modular microfluidics platform

2017 J. Micromech. Microeng. 27 035004

(http://iopscience.iop.org/0960-1317/27/3/035004)

IOP Publishing Journal of Micromechanics and Microengineering

J. Micromech. Microeng. **27** (2017) 035004 (14pp) doi:10.1088/1361-6439/aa53ed

A truly Lego®-like modular microfluidics platform

Kevin Vittayarukskul and Abraham Phillip Lee

Department of Biomedical Engineering, University of California, Irvine, CA, USA

E-mail: aplee@uci.edu

Received 11 October 2016, revised 15 November 2016
Accepted for publication 15 December 2016
Published 24 January 2017

Abstract

Ideally, a modular microfluidics platform should be simple to assemble and support 3D configurations for increased versatility. The modular building blocks should also be mass producible like electrical components. These are fundamental features of world-renowned Legos® and why Legos® inspire many existing modular microfluidics platforms. In this paper, a truly Lego®-like microfluidics platform is introduced, and its basic feasibility is demonstrated. Here, PDMS building blocks resembling 2 × 2 Lego® bricks are cast from 3D-printed master molds. The blocks are pegged and stacked on a traditional Lego® plate to create simple, 3D microfluidic networks, such as a single basket weave. Characteristics of the platform, including reversible sealing and automatic alignment of channels, are also analyzed and discussed in detail.

Keywords: modular, 3D-printing, Lego®, 3D microfluidics, building block, overmold

(Some figures may appear in colour only in the online journal)

Introduction

Microfluidics is a rapidly emerging technology with promising biomedical applications. Essentially, the technology involves fluid manipulation at the microscale, where the fluid is typically actuated via pressure regulators or syringe pumps. Microscale features, such as channels and valves, of a microfluidic device determine the pattern and direction of flow. A typical microfluidic device is much like a piping network, except the pipes have diameters in the submillimeter range.

There are numerous advantages associated with working at the microscale. These include high throughput and integration of multiple operations on a single microfluidic chip. For example, operations such as mixing, filtration, and detection can all be integrated on a single microfluidic device for automated sample analysis [1]. Furthermore, high throughput operations can run on such devices [2].

Using microfluidics, detection of highly dilute compounds, such as rare, blood-borne cancer cells or bacteria, is possible [3, 4]. In addition, the miniaturization enables microfluidic devices smaller than quarters. Compared to traditional methods, these devices also reduce sample volume requirements and hasten sample analysis. Such features are ideal for point-of-care diagnostics [5].

Another auspicious application of microfluidics is *in vitro* modeling of biological systems. Since microfluidics operates at the micro-level, it can effectively recapitulate physiological features relevant at the microscale. As a result, accurate models of human blood vessels and the lung have been fabricated [6, 7]. Such devices are often called tissues- or organs-on-chips, which are revolutionary tools for drug testing and fundamental biology research.

Despite its promising potential, microfluidics essentially remains a niche technology, with a user base predominantly consisting of engineers. Similar to the early computer, a major reason for the low popularity is because microfluidics is complicated, specifically in terms of fabrication, and thus inaccessible to a larger population [8]. A typical fabrication process involves creating a microfluidic design in a CAD program, printing out the design on a high resolution mask, and photolithographically patterning a master mold in a cleanroom. PDMS, the most popular polymer for microfluidics research, is then cast on this master mold to create microfluidic chips. These chips are finally sealed by bonding to a

PDMS or glass substrate via oxygen plasma treatment [9]. In addition to arduous fabrication, these microfluidic devices are also inflexible to design modifications post-production. To increase adoption rate, there is a need for facile, low-cost methods of building microfluidic devices.

One approach, modular microfluidics, refers to microfluidic devices assembled from individual building blocks. Each has a basic, fundamental function. It is comparable to using the same set of alphabet letters to create numerous different words. Therefore, instead of fabricating complete microfluidic devices through, for example, 3D printing or photolithography, complete devices are assembled from a set of pre-fabricated parts. This approach is attractive for non-technical users because no fabrication or design expertise is required. Not only does this versatile microfluidics engineering paradigm obviate onerous fabrication requirements, it also promotes increasingly functional designs having progressively complicated, larger architectures within a common platform. Building blocks can also be reconfigured and customized for new applications and added functionality.

An early modular microfluidics approach was described by Langelier *et al* in 2011 [8]. They fabricated PDMS microfluidic chips in the shape of jigsaw puzzle pieces. The interlocking tabs of the chips allowed them to interface and self-align with one another. This was similar to a platform developed by Hsieh *et al* [10]. However, 3D configurations were not possible in these platforms. Po Ki Yuen *et al* developed a microfluidic breadboard that functioned similar to an electronic breadboard. The breadboard connected the channels of various, 3D-printed microfluidic chips attached to it, just as an electronic breadboard connects the circuit between connected electrical components [11]. Bhargava *et al* 3D printed discrete microfluidic elements that snapped together in 3D. Therefore, in this platform, creating a complete, 3D microfluidic device was comparable to building something out of Legos® [12]. Lee *et al* also employed 3D printing to create discrete building blocks [13]. However, directly 3D printing many building blocks at high resolution is time consuming and becomes increasingly expensive.

Lego®-like building blocks offer design flexibility and facile construction comparable to traditional Legos®. In addition to usability, the recognizability of a Lego®-like platform further appeals to a more general user base. That is why many existing modular microfluidic platforms strive to emulate the traditional Lego® platform. However, the microfluidics platform described in this paper is truly Lego®-like. Here, the building blocks are essentially 2 × 2 Lego® bricks with integrated microfluidic channels, and each are cast from 3D-printed master molds. These fluidic modules are simply and reversibly assembled on a Lego® plate. Similar to traditional Legos®, they are also stackable, and their geometry is favorable for mass production via injection molding. The blocks are composed purely of PDMS. To test the feasibility of this platform, a range of microfluidic Lego-like® blocks were fabricated and used to assemble simple microfluidic systems, including 3D configurations. Various aspects of this platform, including alignment accuracy, 3D printing dimension fidelity, and burst pressure, are characterized and discussed, as well.

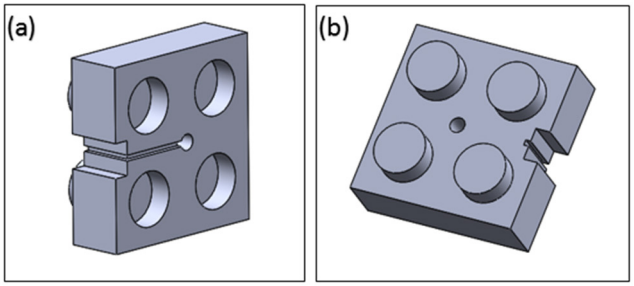

Figure 1. An example of a Lego®-like microfluidic building block. There are microfluidic channels imprinted on the bottom and lateral surfaces.

Materials and methods

Building block design

The general Lego®-like microfluidic block was a cuboid geometrically comparable to that of a traditional 2 × 2 Lego® brick (figure 1). The bottom surface of the cuboid contained 4 stud holes (figure 1(a)). The building block stud holes were designed to have diameters slightly smaller than the stud diameters of a traditional Lego® plate, which are nominally 4.9 mm. For a given block, the nominal stud hole diameters, or the diameters defined in AutoCAD, were either 4.65 mm or 4.8 mm. As a result, an interference fit was formed at the stud connections during block assembly. Building blocks were also designed to have 4.9 mm diameter studs on their top surfaces, enabling block stacking.

Protruding tabs (inward and outward) were designed at the lateral edges of discrete blocks (figure 2). Consider a building block pegged on a Lego® plate. The effective linear interface length (ELIL) is defined as the perpendicular distance from a block lateral surface—or tip of a protruding tabs—and the adjacent studs holding the block. The ELIL of each block extended such that they theoretically overlapped with the ELIL's of adjacent building blocks in an assembly. Physically, this caused block lateral surfaces to press against neighboring lateral surfaces with a pressure that scaled with amount of overlap. The protruding tabs localized the block lateral interfaces to a smaller lateral surface area. This is compared to a block lateral interface without protruding tabs. Therefore, the pressure at such interfaces was increased for a given overlap distance. In addition, the smaller surface area of contact reduced the likelihood of seal-compromising defects. In this paper, the amount of overlapping distance ranged from roughly 20 μm–300 μm.

All microfluidic channels had a nominal cross-sectional width and height of 500 μm. Microfluidic channels were imprinted on the building blocks' bottom surfaces (figure 1). As seen in figure 3, to form 2D microfluidic networks, channels on the bottom surfaces of adjacent building blocks interfaced with each other at the block edges. The Lego® base plate or a building block's top surface sealed these channels. 3D configurations were realized with channels that perpendicularly extended from bottom surface channels. These channels were either biopsy punched at the top surface or were imprinted

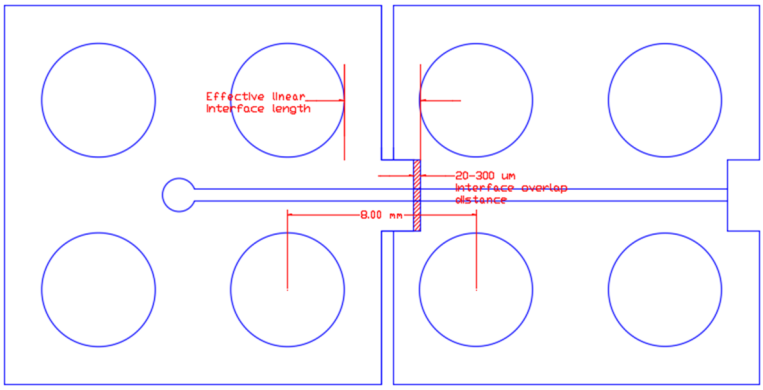

Figure 2. A 2D sketch of 2 building blocks interfaced with each other. ELIL and interface overlap are depicted.

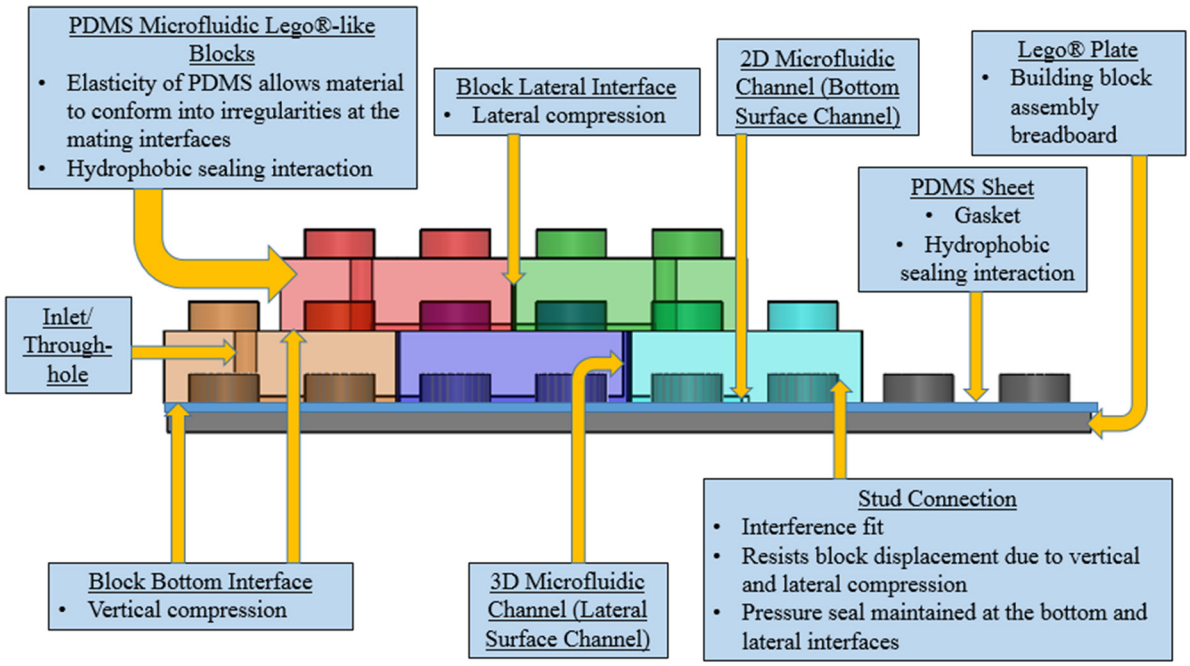

Figure 3. A side-view of a building block assembly on top of a Lego® base plate.

on the lateral surface of a building block (figure 1). Lateral surface channels terminated at the top surface of the building block it belonged to, and the lateral surface of an adjacent building block sealed these channels. Lateral surface channels connected to bottom surface channels of building blocks stacked directly on top. Inlets and outlets were created by punching through-holes with a biopsy punch.

Fabrication of master molds

Individual PDMS microfluidic building blocks were cast from master molds. To begin, each master mold was designed two-dimensionally in AutoCAD, and 3D features were extruded in Solidworks. Overhangs were deliberately omitted from the design. A resulting 3D CAD model was 3D printed using a Perfactory 3 Mini 3D printer (EnvisionTEC). The material used in this machine was R5 Gray (EnvisionTEC). The ULTRA 3SP 3D printer (EnvisionTEC) was also used. Here, the material polymerized was ABS 3SP Flex Gray (EnvisionTEC). Both printers employ digital light processing (DLP), a highly accurate method of 3D printing.

The material used in these DLP 3D printers inhibited PDMS curing. Therefore, the original 3D-printed master molds were recast with a material compatible with PDMS casting. To begin, the negative impression of an original master mold was cast using tin-based silicone (TC-5024, BJB) at a 10:1 weight ratio of base to crosslinker. The silicone was allowed to cure at room temperature for 6 h. After the silicone mold cured, liquid plastic (Smooth-Cast 310, Smooth-On) was poured onto the negative impression. The liquid plastic was cast at a 1:1 volume ratio of Part A to Part B and cured at room temperature for 3 h. The liquid plastic became rigid once cured, resulting in a urethane version of the 3D-printed master mold. Next, a negative impression of the urethane master mold was cast with PDMS (Sylgard 184, Dow Corning). PDMS was mixed at a 10:1 weight ratio of base to crosslinker and cured at 60 °C for 3 h. This PDMS casting was oxygen plasma treated for 2 min and followed by overnight silane treatment [14]. Afterwards, a PDMS version of the urethane master mold was cast from the PDMS negative impression casting. The resulting PDMS master mold was also silane treated.

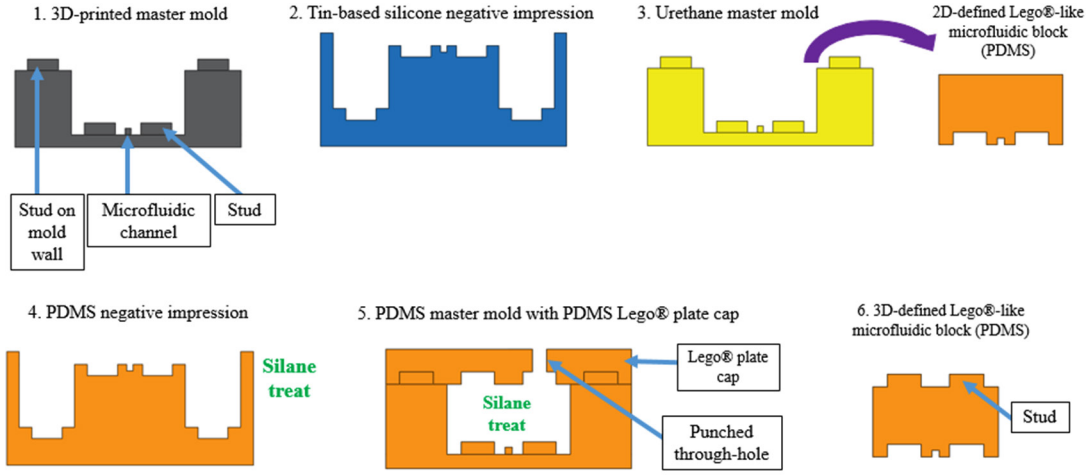

Figure 4. A cross-sectional side view of the fabrication process for a single building block.

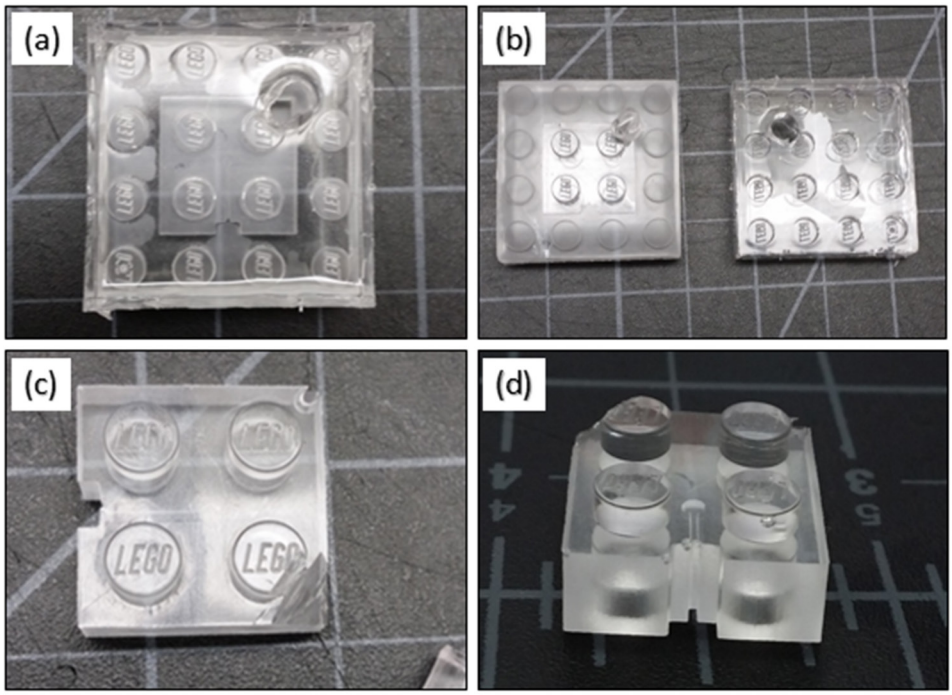

Figure 5. The fabrication process of 3D-defined building blocks. (a) A PDMS master mold capped by a PDMS Lego® plate cap. Degassed PDMS is introduced into the top right hole. (b) An uncapped PDMS master mold with an unremoved building block (left) and a PDMS Lego® plate cap (right). (c) A 3D-defined block with its defect cut off. (d) A 3D-defined block.

A 4 stud × 4 stud Lego® mold was constructed on top of a traditional Lego® plate using ordinary Lego® bricks. From this cavity, a 4 stud × 4 stud negative impression of the Lego® plate was cast using PDMS. A hole was punched near the corner of this PDMS Lego® plate cap using a 5 mm biopsy punch. The punched hole slightly overlapped with one of the stud holes (figure 5(b)). The cap was then silane treated. To conveniently generate multiple PDMS Lego® plate caps, liquid plastic was poured over the cap in a container. The cured plastic became a master mold for the PDMS Lego® plate cap.

The PDMS Lego® plate cap was snapped onto the studs that protruded from the top of the PDMS master mold walls. The stud connections each formed an interference fit because the diameters of the cap stud holes were slightly smaller than the master mold wall stud diameters, which were nominally 5.1 mm. The combined cap and master mold formed a cavity defined in all 3 dimensions. Figure 4 summarizes the master mold fabrication procedure.

Fabrication of building blocks

To cast a microfluidic building block, PDMS was poured into a urethane master mold and cured. Because master molds did not contain overhangs, there was no obstruction to the vertical removal of cured building blocks. Therefore, they were simply pried out of the molds using a blunt knife or tweezers. Building blocks fabricated in this method were not 3D-defined and did not have protruding studs on their top surfaces (figure

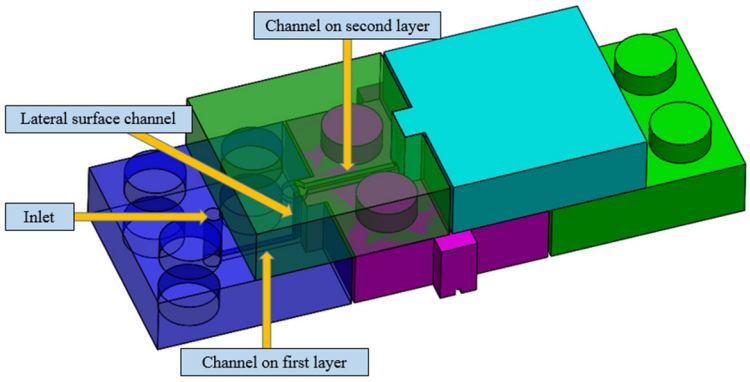

Figure 6. Lateral surface channels connect the bottom surface channels for 3D microfluidics. The assembly is composed of 2 layers of building blocks. The purple block's (bottom middle) sidewalls seal the lateral surface channels on the blue (bottom left, shown) and green block (bottom right, hidden).

4, step 3). They could only be used for single layer, 2D microfluidic configurations.

In order to stack discrete blocks, dimensions defined in 3D were required. 3D-defined building blocks differed from the aforementioned Lego®-like microfluidic blocks by having defined heights and protruding studs on the top surfaces (figure 4, step 6 and figure 5(d)). These were cast from the combined PDMS cap and master mold (figure 4, step 5). Through the hole previously punched in the Lego® cap, degassed PDMS was introduced into the cavity (figure 5(a)). Since the Lego® plate cap and PDMS master mold were both silane treated, the cured PDMS microfluidic Lego®-like block was easily removed by flexing the master mold. An unavoidable defect was present on the resulting building block due to pouring PDMS through the punched hole. Thus, a knife was used to cut the unwanted structure off at an angle, leaving functional structures uncompromised (figure 5(c)).

Assembly of a complete microfluidic device

A complete, sealed microfluidic device was created by attaching a set of building blocks onto a Lego® plate (figure 3). A given block in a microfluidic device assembly experienced vertical compression at its block bottom interface. Because the blocks were designed to have overlapping ELIL's in an assembly, the block lateral interfaces experienced lateral compression, as well. In the first layer of blocks, a pegged block's stud holes formed an interference fit with the Lego® plate studs. Blocks on higher layers formed an interference fit with the studs protruding from the top surface of blocks directly below them. As a result of the interference fits, blocks resisted displacement due to the compression forces on them, and a pressure seal was maintained at the block bottom and block lateral interfaces. Furthermore, the studs positioned microfluidic channels of interconnected chips such that they were automatically aligned. 2D networks or layers expanded with addition of adjacent building blocks, and 3D configurations extended by stacking additional building blocks.

Using a CO_2 laser cutter (VersaLaser, Universal Laser Systems), a 1 mm-thick PDMS sheet was laser cut into the shape of a Lego® plate. Through holes were cut at the stud positions. The laser settings were 40% power, 10% speed, and 1000 PPI. This laser-cut PDMS sheet was laid on top of the traditional Lego® base plate. Therefore, all mating interfaces were PDMS surfaces pressed against each other. By being able to conform to surface irregularities under pressure, the elasticity of PDMS assisted in both lateral interface and bottom interface sealing. In addition, the hydrophobic PDMS–PDMS sealing interactions helped against leaking. Multimedia S1 demonstrates an example of constructing and using a microfluidic assembly.

2-layer assembly: a single basket weave. A 2-layer, basket weaving configuration was assembled by first creating a straight channel with 3 building blocks, 2 inlets and 1 straight channel block. 2 additional inlet blocks were connected to the remaining, unoccupied sides of the middle block. This assembly represented the first layer. The middle block was a 3D-defined block and also contained 2 punched through-holes that linked to channels on its bottom surface. Finally, a resistor channel block was appended on the top of the middle block. The resistor channel connected both of the punched through-holes. Dyed water was flowed through the channels and used to detect any leakages.

2-layer assembly: lateral surface channels. To demonstrate sealing of lateral surface channels by adjacent block walls, a 2-layer device was assembled. The first layer of the assembly consisted of a 3D-defined straight channel block between 2 3D-defined blocks with lateral surface channels. The 2 lateral surface channels were sealed by the adjacent walls of the 3D-defined straight channel block. 2 inlet blocks were then stacked on top of these blocks, and their bottom surface channels connected to the lateral surface channels rising from the first layer. Figure 6 highlights how a lateral surface channel is sealed and connects bottom surface channels on separate layers.

3-layer assembly. A 3-layer assembly was also created. The first layer configuration was the same as in the methods section, '2-layer Assembly: Lateral Surface Channels'. The second layer consisted of an inlet block that connected to a lateral

surface channel from the first layer. The second layer also contained a 3D-defined block containing 2 punched through-holes. Finally, a resistor block was stacked on top of the aforementioned block, and this formed the third layer.

2D alignment accuracy and repeatability

For a given interface overlap amount, 2 straight-channel or inlet blocks were assembled in series. Then, a microscope (Eclipse TE2000-S, Nikon) was used to visualize the channel interface. Images were taken with a digital camera (Phantom v310, Vision Research). This procedure was repeated 5 times for each of a range of interface overlap amounts. Visual aids were not used during assembly. To assess 2D alignment repeatability for a given overlap amount, the same exact block interfaces were considered for each of the 5 trials. To quantify 2D alignment accuracy, the midpoints of the channels of each block were considered. The reason being, channel widths varied from block to block due to 3D printing limitations. In ImageJ, a line was used to connect the 2 midpoints, and another line was perpendicularly drawn from a channel wall to its corresponding midpoint. The angle formed by these 2 lines was then measured in ImageJ. A 90° angle represented perfect alignment.

Block edge lift and surface roughness

The edges of individual building blocks attached to a Lego® base plate were examined using microscopy, and the edge lift distances were quantified with ImageJ. The type of 3D printer employed and the size of the block stud hole diameter were compared. 4 different edges were considered for each condition. In addition, the flatness of the edge area of urethane master molds was measured with a 3D laser scanning microscope (VK-X100, Keyence). Master molds derived from the ULTRA 3SP and Perfactory Mini 3D printers were compared, and 5 different samples were considered for each condition. The arithmetic mean surface roughness of building blocks was also quantified using the Keyence. Blocks derived from the ULTRA 3SP and Perfactory Mini 3D printers were again compared. Further, the surface roughness of a microfluidic device cast from a silicon wafer master mold was measured for additional comparison.

Dimension fidelity

Building blocks were attached on a Lego® base plate, and microscope images were taken of various features. Measurements were made using ImageJ and used to determine block ELIL's. Microscope images were also taken of building block stud hole diameters, while the blocks laid on top of a flat glass slide. Again, ImageJ was used to quantify the dimensions. 6 samples were considered for each of the aforementioned conditions. Channel width, height, and sidewall taper angle of urethane master molds were measured using the Keyence 3D laser scanning microscope. For each of these conditions, 3 different samples were measured. The dimension fidelity of each 3D printer used was compared. Digital calipers (ABSOLUTE Digimatic, Mitutoyo), were used to measure 4 different stud diameters of a traditional Lego® plate.

Burst pressure for different interface overlap amounts

For a given interface overlap amount, 2 inlet blocks were assembled in series. The blocks in this test had nominal stud hole diameters of 4.8 mm. Using pressure regulators (ITV0011-2UMS, SMC), the device was primed with dyed water at a 0.16 psi source pressure. Then, the source pressure was reduced to 0.064 psi, and the outlet was taped over. A device assembly was defined as successful if it held the 0.064 psi source pressure for 1 min. This time frame was sufficiently long to eliminate many leakage instances due to variables, such as poor building block placement or set up, not being tested. If a device was successful, the pressure in the device was increased by 0.01 psi increments until leakage was observed. Each increment in pressure was held for 1 min. Only the burst or leakage pressures of successful devices were recorded, and 3 burst pressures were obtained for a given overlap amount. This procedure was repeated until burst pressures were obtained for a range of interface overlap amounts.

Burst pressure for different numbers of blocks in series

A random set of building blocks were used to assemble n blocks in series, where $n = 1, 2, 3,$ or 4. The blocks in this test had nominal stud hole diameters of 4.8 mm. The block in the 1-block condition was a self-contained resistor channel block. Interface overlap amounts were not accounted for. The reason being, each building block had unique dimensions due to the variable nature of 3D-printed objects. Therefore, constant interface overlap amounts could not be achieved as n varied. The burst pressures for each set of blocks were obtained using the procedure described in the methods section, 'Burst Pressure for Different Interface Overlap Amounts'.

Burst pressure for different interference fits

To test the effect of interference fit strength on burst pressure, the burst pressure of a self-contained resistor channel block with nominal stud hole diameters of 4.8 mm was determined. Separately, the burst pressure of another self-contained resistor channel block with nominal stud hole diameters of 4.65 mm was obtained. The burst pressures were obtained by following the procedure described in the methods section, 'Burst Pressure for Different Interface Overlap Amounts'.

Results and discussion

3D microfluidic assemblies

Leak-free, 3D assemblies consisting of stacked PDMS microfluidic blocks were demonstrated. In figure 7, a simple basket weaving configuration is shown. Red water flowed in a

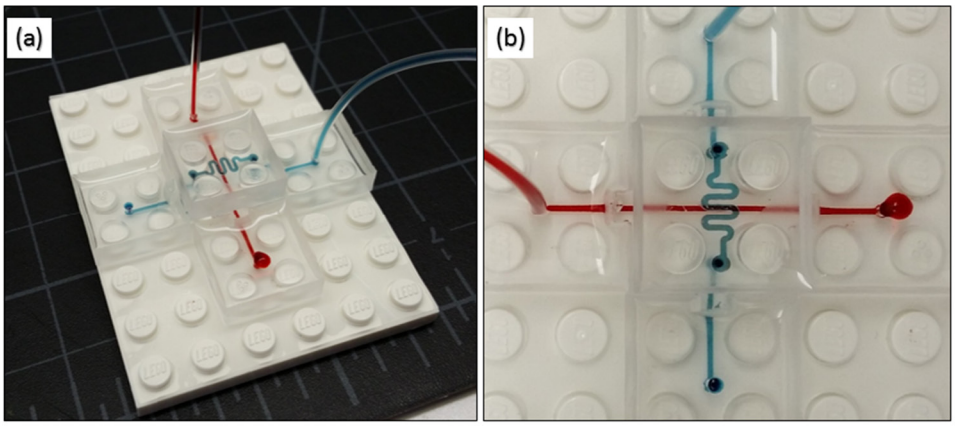

Figure 7. A single microfluidic basket weave with 2 layers of blocks. (a) An angled view from the top. (b) A top-down view. No leakages are visible.

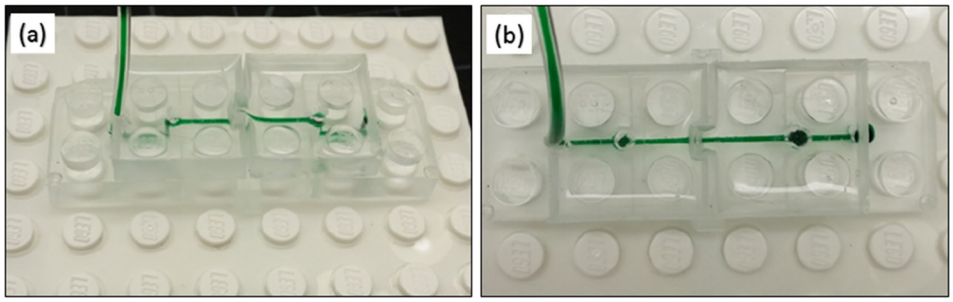

Figure 8. A 2-layer assembly using lateral surface channels to connect both layers. (a) An angled view from the top. (b) A top-down view. No leakages are observed.

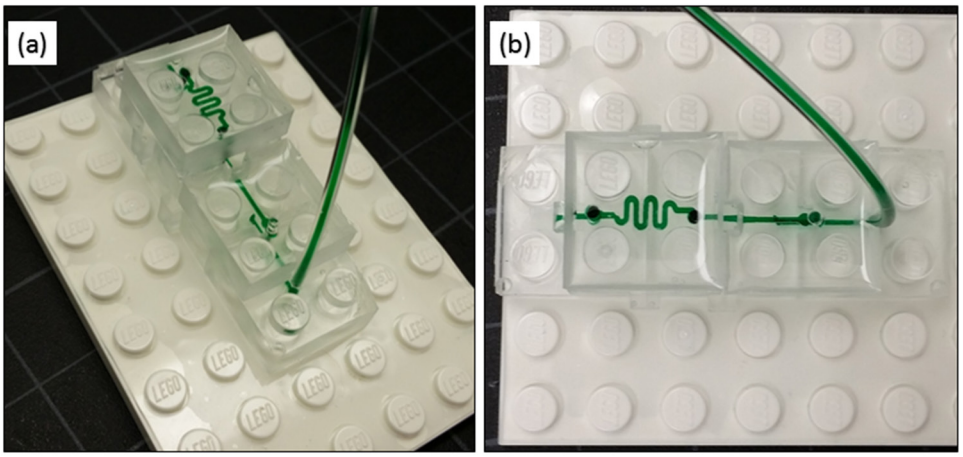

Figure 9. A 3-layer microfluidic assembly. (a) An angled view from the top. (b) A top-down view. The device is leak-free.

straight channel on the first layer. Blue water flowed over by connecting to the second layer. It connected through punched holes in the middle block of the first layer. No leakages were observed. Multimedia S2 shows fluid flow in this device.

Figure 8 validates lateral surface channel sealing using a neighboring lateral surface. It also demonstrates successful 2D block interfacing using the top surface of building blocks rather than the traditional Lego® base plate. Both of these results are fundamental requirements for creating increasingly intricate microfluidic networks in 3D. Finally, a 3-layer 3D microfluidic assembly was proven (figure 9). In an assembly, it becomes increasingly difficult to avoid leakages as more building blocks are stacked. There is simply more room for errors leading to leaks. This result pushed the limit of how many layers can currently be achieved. It showed that at least 3 was possible. Ultimately, although the results demonstrated are simple, they validate a foundation that can be employed for facilely building more complex microfluidic systems.

2D alignment accuracy and repeatability

The 2D alignment accuracy of a building block lateral interface for different interface overlap distances is plotted in figure 10. These results characterized the automatic alignment

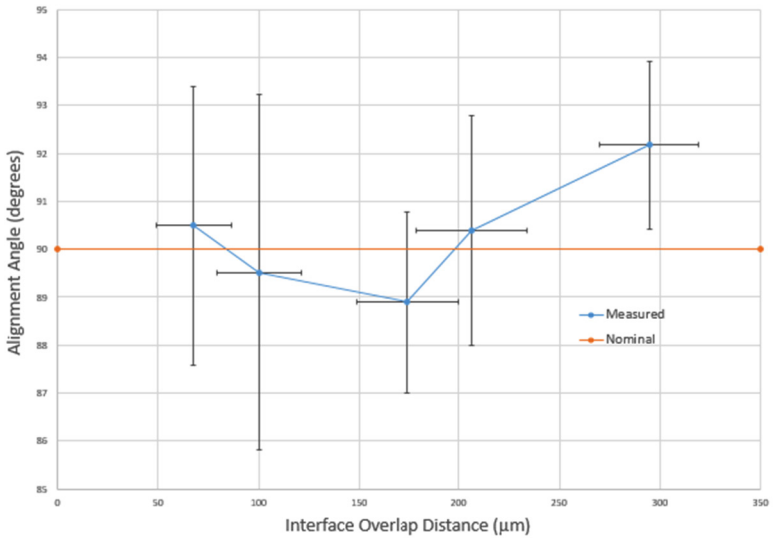

Figure 10. A graph of alignment accuracy and repeatability. The average alignment angle of an interface is shown for different interface overlap distances (blue line). Error bars depict standard deviation. A 90° angle represents perfect alignment (horizontal orange line).

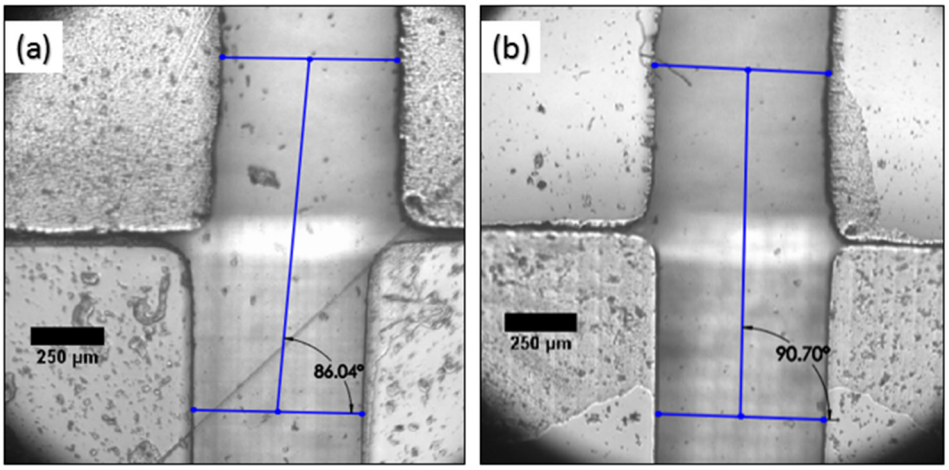

Figure 11. Microscope images of the interface of 2 building blocks. The blue lines demonstrate how alignment angle is determined. (a) Poor alignment. (b) Good alignment. The scale bar is 250 μm.

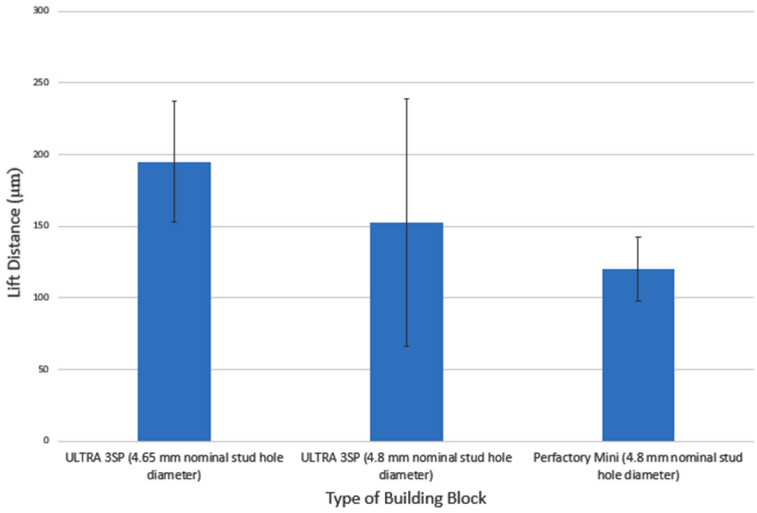

Figure 12. A bar graph of edge lifts for different building blocks on top of a Lego® base plate. Error bars represent standard deviation.

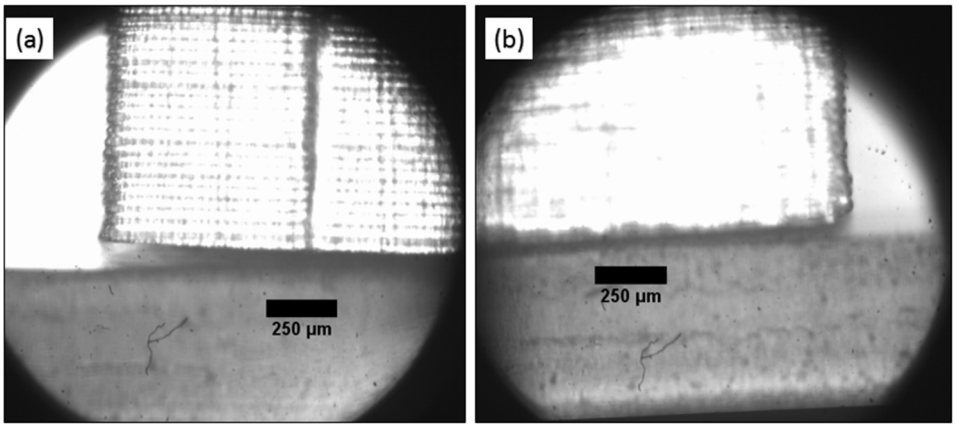

Figure 13. Microscope images of edge lifts of blocks on top of a Lego® base plate. (a) Max edge lift is about 100 μm. (b) Minimum edge lift is about 37.5 μm. The scale bar is 250 μm.

ability of stud connections. The average alignment angles deviated slightly from the horizontal line representing an ideal 90° alignment angle. Poor alignments were off by about a few degrees, depicted in figure 11(a). Outstanding alignment is shown in figure 11(b). The highest deviation seemed to occur with highest overlap amount. A possible explanation is that under the increased pressure, the lateral interface surfaces shifted horizontally (to the left or right) for relief.

The straightness and positioning fidelity of the channels likely exacerbate alignment angle deviations from the ideal 90°. For example, a straight channel slightly tilted in the horizontal plane would add to alignment angle deviation. Now consider a situation where 2 interconnected, straight channels are perfectly parallel with respect to each other. If the positioning of the channels was off, the line connecting the channels' midpoints would angle away from 90°. Unfortunately, these limitations are often inherent in 3D printing technology.

For channel widths roughly or greater than 500 μm, the 2D alignment accuracy is sufficient. For much smaller channels, smaller deviations become increasingly critical. If initial alignment is off, accuracy can be improved within a few, simple reattachments or readjustments of the concerned blocks. In addition, higher quality master molds, such as accurately micro-machined molds, may improve alignment accuracy results.

The error bars in figure 10 represent the standard deviations of the measurements and thus characterize the repeatability of automatic alignment. The standard deviations were quite large and did not significantly vary with overlap distance. The high standard deviations may be attributed to the high elasticity of PDMS. This material can easily deform or shift under the pressure at the lateral interface or during building block assembly. The large length of the protruding tabs, nominally 1.6–1.65 mm, may also play a role. As they increase in length, their range of motion should become more independent of their bulk building block. Consequently, the alignment guidance provided by the stud connections would have less influence the tabs' positions. These factors can explain alignment variation about a mean alignment angle. Therefore, repeatability could increase with stiffer blocks and shorter protruding tabs.

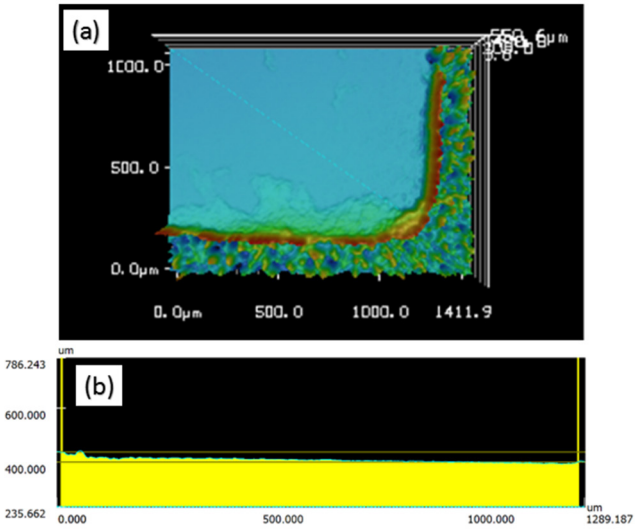

Figure 14. (a) 3D surface topography of a master mold corner. (b) The surface height along the dotted blue line in (a).

Block edge lift and surface roughness

The bottom interfaces of building blocks placed on a Lego® base plate were not completely sealed. The edges of the blocks vertically lifted off of the Lego® base plate surface. The average lift distance is shown in figure 12. Block edge lift is likely the largest reason for this platform's low burst pressure, which will be discussed later. It creates a large gap at the block bottom interface for fluid in microfluidic channels to escape through. Blocks from the ULTRA 3SP printer with nominal stud hole diameters of 4.65 mm had the highest average edge lift. Blocks from the same printer but having larger stud hole diameters had a lower average in comparison. The lowest average block edge lift was measured on blocks from the Perfactory Mini and having 4.8 mm nominal stud hole diameters.

An assembly of building blocks that immediately leaks before any pressure is held was defined as unsuccessful. Whether a device is successful or unsuccessful is likely very dependent on the block edge lift near the block lateral interfaces. When an unsuccessful assembly leaks, the lift should be

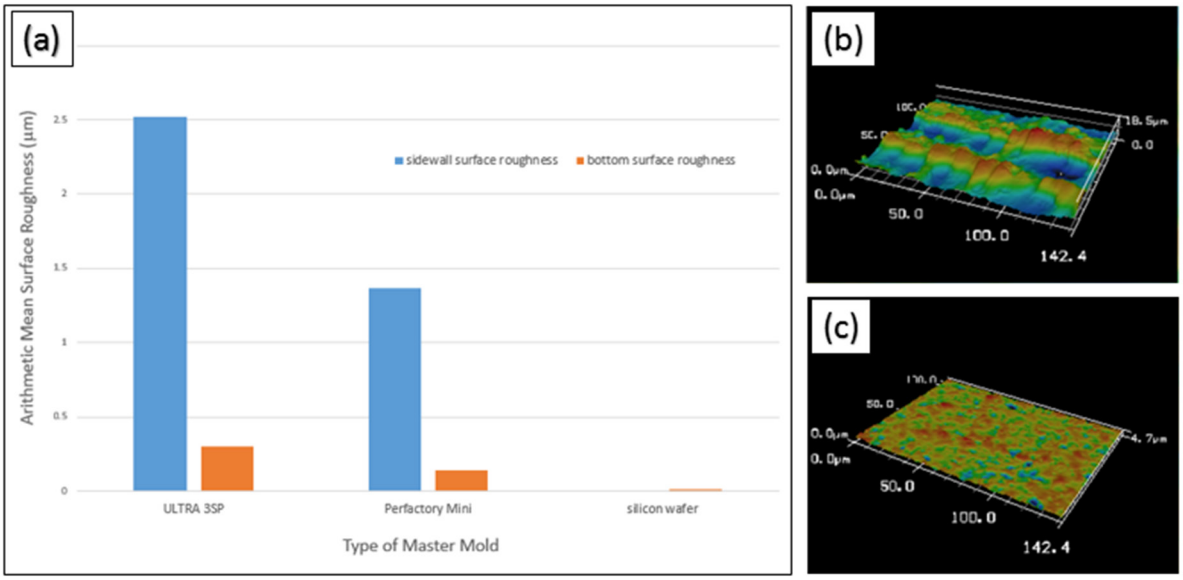

Figure 15. (a) A bar graph of building block surface roughness from different master molds. (For each category, bars on left refer to sidewall surface roughness.) (b) 3D topography of sidewall surface of an ULTRA 3SP block. (c) 3D topography of bottom surface of an ULTRA 3SP block.

high. For example, the block edge lift in figure 13(a) is about 100 μm. Relatively low edge lift distance, about 37.5 μm in figure 13(b), is likely a good indication that an assembly will be successful.

Blocks with nominal stud hole diameters of 4.65 mm were expected to have lower edge lifts compared to blocks with larger diameters. The reason being, smaller stud hole diameters would result in stronger interference fits at stud connections. Therefore, there should be improved resistance to vertical displacement at the block bottom interface. The current results may suggest that the tighter the interference fit, the less likely the fit will be held. That is, it is more difficult for a block to be completely inserted into protruding studs if the stud connection fit is too tight. However, when the block does completely peg onto the protruding studs, the interference fit would be stronger compared to blocks with larger stud hole diameters.

The minimum edge lift is determined by the inherent unevenness of master molds at their bottom surface edges (figure 14). Near the bottom surface edges, edge lift was detected by 3D laser scanning. On average, the edge lift of master molds from the ULTRA 3SP was 28.57 $\pm$ 19.10 μm. The average edge lift of Perfactory Mini master molds was 17.72 $\pm$ 9.573 μm. These results may explain why edge lift of Perfactory blocks on top of a Lego® base plate was on average lower than 3SP blocks. These results are also in line with the lower edge lifts observed for a block attached on a Lego® base plate.

The average edge lift of blocks pegged on a Lego® base plate was much higher than master mold edge lifts. This can be explained by the high elasticity of PDMS. The interference fit at the stud connections may cause the blocks to deform and lift at the edges. Therefore, stiffer blocks may reduce this undesirable edge lift effect. Edge lift could be further reduced if master molds had more even surfaces.

Figure 15 depicts the average surface roughness of PDMS castings from different master molds. The surface roughness of building blocks from 3D-printed master molds is much higher than the average surface roughness of a PDMS microfluidic device casted from a silicon wafer master mold. Perfactory Mini blocks had a lower surface roughness than ULTRA 3SP blocks, especially when comparing sidewall surfaces. For all building blocks, the sidewall surface roughness is significantly higher than the bottom surface roughness. High surface roughness would prevent complete contact of mating interfaces and thus reduces sealing strength. This is especially an issue for block lateral interface strengths. With smoother and more level surfaces, sealing strengths may have at least withstood 3–4 psi of pressure [15]. Unfortunately, rough and uneven surfaces are inherent in 3D-printed objects.

Dimension fidelity

Figure 16 compares the dimension fidelity of blocks from the Perfactory Mini and the ULTRA 3SP. The actual ELIL's of 3SP blocks were quite close to their nominal dimensions. On average, the ELIL's were about 10 μm larger than theoretical values. On the other hand, the measured ELIL's of blocks from the Perfactory were on average about 65 μm short of their theoretical dimensions. Nonetheless, several of overlap distances in the range of 20 μm–300 μm were obtained and studied in this paper.

The stud diameter deviation was also large. 3SP blocks had average stud hole diameters roughly 30 μm greater than expected. Worse, Perfactory blocks had average stud hole diameters nearly 90 μm larger than what they should have been. The stud diameters of a traditional Lego® plate were on average 4.90 $\pm$ 0.005 77 mm. Therefore, despite the deviations, interference fits at the stud connections were still

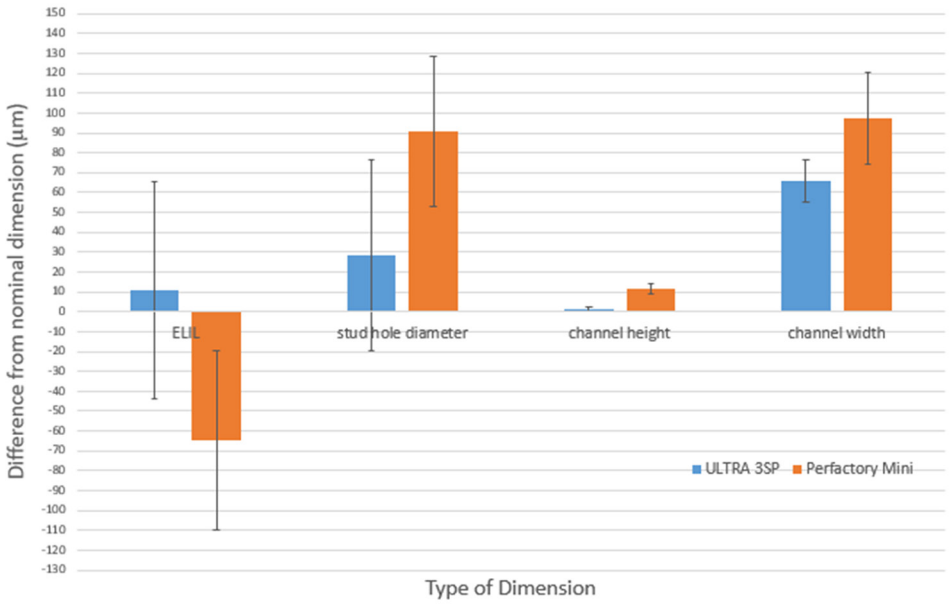

Figure 16. A bar graph of dimension fidelity for various dimensions. Blocks from ULTRA 3SP and Perfactory Mini are compared. (For each category, bars on left refer to ULTRA 3SP.) Error bars show standard deviation.

obtained; they were just weaker than expected. This was especially true for Perfactory blocks. (This loose fit may explain why edge lift of Perfactory blocks on top of a Lego® base plate was on average lower than 3SP blocks.) Besides, it is later shown that the difference in burst pressure for different stud diameters was not significant.

Concerning channel dimensions, the 3SP was also more reliable than the Perfactory. Both printers produced channel heights close to their theoretical dimensions. For the 3SP, the average additional height was only about 1.4 μm. For the Perfactory, it was about 11.4 μm more. Dimension deviation was much greater for channel width. The 3SP added on average about 65.9 μm. On average, the Perfactory added 97.5 μm to the nominal width.

Sidewall taper angle is the angle that the channel sidewall makes with respect to the bottom surface of the master mold. Again, the 3SP was more consistent than the Perfactory. For the 3SP, the mean sidewall taper angle was 87.5 $\pm$ 0.499°. For the Perfactory, the mean sidewall taper angle was 85.2 $\pm$ 1.35°. Figure 17 depicts an example. Although many factors, such as condition of printer and type of resin used, may influence dimension fidelity, these data can inform baseline compensatory adjustments at the CAD level. 3D printing repeatability remains a concern, however.

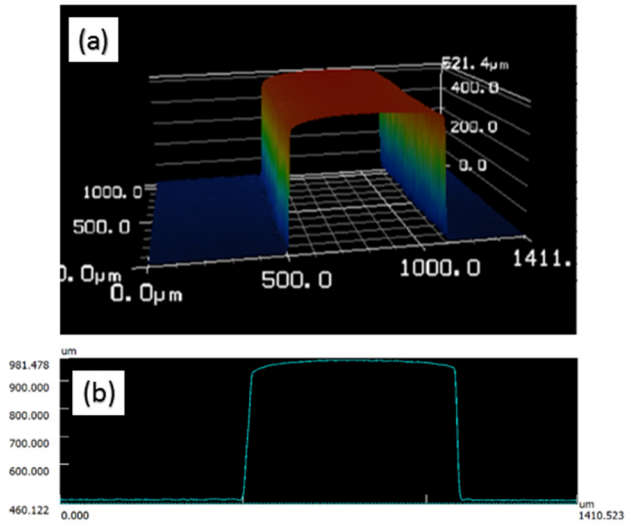

Figure 17. (a) A 3D display of a laser-scanned channel of a 3SP master mold. (b) A cross-sectional profile of the channel in (a).

Burst pressure for different interface overlap amounts

From the graph in figure 18, burst pressure increases for larger interface overlaps but levels off as overlap amount furthers. During the burst pressure tests, the occurrence of leakage was always near the bottom edge of the block lateral interface. Therefore, the burst pressure for a given overlap distance depended, in part, on the robustness of the lateral interface seal. The average burst pressure for a very small overlap, about 20 μm, was 0.12 psi. Increasing, the overlap to about 150 μm–200 μm also increased the burst pressure by about 0.01 psi. However, further increasing the overlap distance did not appear to increase the device burst pressure.

Burst pressure initially increases with overlap amount, suggesting that higher overlap amounts resulted in higher pressure seals at the lateral interface. However, as overlap distance further increased, the burst pressure leveled off. This suggests that too much lateral interface pressure begins to counteract the seal strength. Under increased pressure, the interface is more prone to deform and shift, not just horizontally but vertically, as well. In addition to block edge lift, additional vertical displacement at the lateral interface would significantly reduce burst pressure strength.

It also is apparent that the general burst pressures for this platform are very small, roughly 0.11 psi–0.13 psi. This is

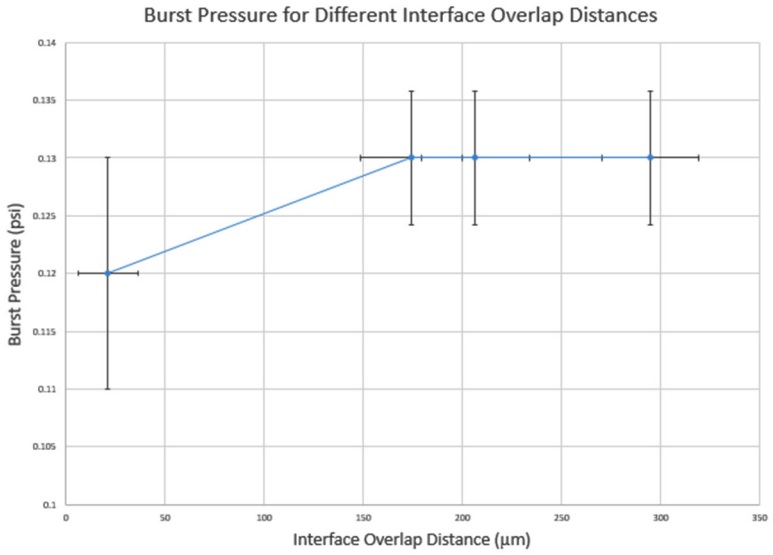

Figure 18. A graph of burst pressure for different interface overlap distances. Error bars represent standard deviation.

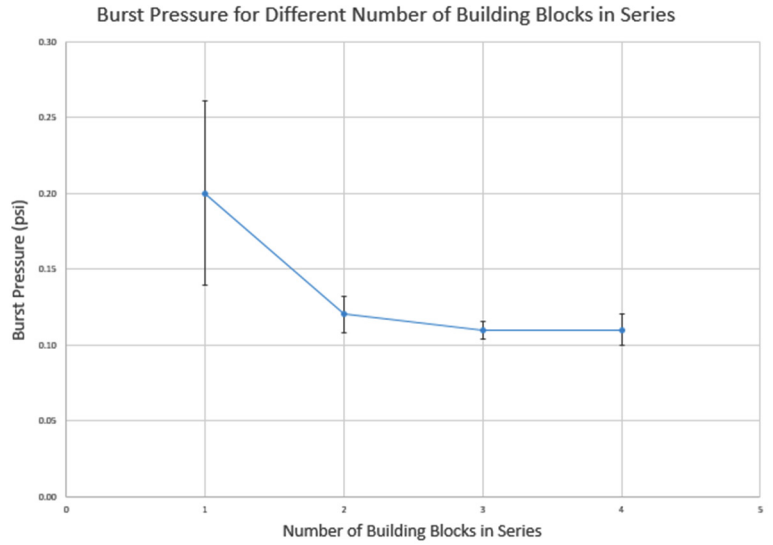

Figure 19. A graph of burst pressure for different numbers of building blocks in series. Error bars represent standard deviation.

expected given all the factors that can compromise a strong interface seal: block edge lift, high sidewall surface roughness, and interface shifting under pressure. These factors may also explain the lack of a more obvious or significant trend as overlap amount increases. For example, leakages may occur due to these universal issues before the strengths of the pressure seals are fully tested. Thus, noticeable differences in burst pressures would not be realized. Furthermore, in this range of pressures, there may be differences in burst pressures that are too small to be discerned with the equipment used.

Burst pressure for different numbers of blocks in series

The graph in figure 19 depicts how burst pressure varied as more blocks were added in series. Leakage for the single block always first occurred under the inlet. When leakage occurred for assemblies containing 2 or more blocks, it was always at the bottom edge of a block lateral interface. When there was more than one lateral interface, the first sign of leakage only occurred at one of the interfaces. According to the graph, burst pressure was highest for 1 block and dropped as the number of blocks increased. Burst pressure for 2 blocks was slightly higher than 3- and 4-block assemblies, both of which had similar burst pressures.

The burst pressure for 1 block was significantly higher than for multi-block assemblies because it had no lateral interfaces. The single block only contained channels on its bottom surface. Therefore, burst pressure for $n = 1$ represents the sealing strength of the block bottom interface. For a few reasons, the block bottom interface of a 1-block system should be stronger than a lateral interface. First of all, the bottom interface will not shift under lateral pressure. It also has a smoother surface, and block edge lift is less drastic towards block centers. Unsurprisingly, burst leakages always initiated at the inlet, which was the part of the channel closest to the block edge.

The burst pressure results for multi-block assemblies do not appear to significantly differ from the results for the 2-block assemblies in the results section, 'Burst Pressure for Different Interface Overlap Amounts'. This suggests that the strength of a given lateral interface seal is not highly affected by the number of blocks in an assembly. However, the drop in burst pressure from 2 to 3 blocks suggests that adding more blocks compromises lateral interface seal strength. For example, increasing the number of blocks in an assembly adds to the overall stress in the entire system. This may propagate interface deforming and lifting effects. On the other hand, the difference in burst pressure from 3 to 4 blocks suggests otherwise. Here, the average burst pressures did not differ, and the 4-block assembly even had larger max burst pressures.

For 3- and 4-block assemblies, burst leakage initiated at only one of the multiple lateral interfaces. The compromised interface likely represents the weakest link—or the weakest lateral interface. Therefore, if the weakest link bursts first, the burst pressure of an entire assembly is totally dependent on the weakest link. It is then plausible that as n increases, the likelihood of including a weaker link increases. This explanation is in agreement with lateral interface seal strengths not being greatly affected by adding more blocks.

Burst pressure for different interference fits

The single block with nominal stud hole diameters of 4.65 mm had a burst pressure of 0.21 ± 0.071 psi. When the nominal stud hole diameters increased to 4.8 mm, the burst pressure was 0.20 ± 0.061 psi. These burst pressure results indicate the strength of the block bottom interface. Therefore, these results suggest that stronger interference fits increase the sealing strength of block bottom interfaces. This is expected since a stronger interference fit better resists displacement due to vertical compression. Thus, a higher pressure seal can be maintained.

There are 2 possible explanations for the minor difference in burst pressure. First, the stud hole diameters compared were not sufficiently different. As a result, the difference in strength of the respective interference fits could be minor. Or, the blocks prematurely leaked due to other factors, such as block edge lift, before noticeable differences were realized.

Potential ways to improve platform efficacy and function

It was discussed that the low burst pressures of this platform may be attributed to interface shifting under pressure, block edge lift, and high surface roughness. It was suggested that stiffer building blocks may be one way to improve burst pressure. One approach would be to cure PDMS at a higher temperature and/or increase the crosslinker to base weight ratio [16].

Another possible solution would be the use of overmolded blocks. In an overmolded block, the bulk core of the block is a rigid material, such as acrylic. The core is surrounded by a thin, rubbery layer, such as PDMS. As a result, the block would be rigid but still enable gasket seals at the interfaces. Theoretically, the interference fits and interface pressure seals would be much stronger compared to pure PDMS blocks, as well. An overmolded block may be fabricated by inserting a laser-cut acrylic core into a PDMS master mold and pouring PDMS over it. The size of the core should be such that there is some inter-wall gap between itself and the master mold walls (figure S1). The flexible PDMS master mold would facilitate the release of the rigid overmolded block once cured. At an industrial scale, overmolded blocks can be injection molded. If reversibility is not a concern, the stamp-and-stick method could potentially solve this platform's issue of low burst pressures [17]. In addition, if the current block surfaces were smoother, an assembly could be plasma bonded together.

Due to the presence of studs, another limitation of the platform is restricted real estate for microfluidic features. To increase functional surface area, stud diameters may be reduced. Their geometry can also be designed to minimize footprint. One strategy is a semi-cylindrical stud shape. Positioning studs further towards building block corners increases space for microfluidic structures, as well.

Conclusion

A truly Lego®-like microfluidics platform circumvents the alienating fabrication requirements of traditional microfluidic devices. Here, creation of custom, 3D microfluidic devices is really as simple as assembling traditional Legos®. The Lego®-like design is simple, usable, and promotes mass production. These features should encourage a broader range of researchers to adopt the promising technology of microfluidics. The results of this research demonstrate a proof-of-concept for a truly Lego®-like microfluidics platform. This paper characterized the platform's features, such as its reversible pressure seal and automatic alignment. It also discussed approaches to improve these aspects. For example, overmolded blocks and smoother master molds with more even planes were suggested. Crucially, this research lays the foundation for further optimization of a truly Lego®-like microfluidics platform.

Acknowledgments

This research was supported by a grant from the UCI Undergraduate Research Opportunities Program (UROP). Lego® is the registered trademark of The LEGO Group.

References

[1] Hughes A J, Lin R K, Peehl D M and Herr A E 2012 Microfluidic integration for automated targeted proteomic assays *Proc. Natl Acad. Sci. USA* **109** 5972–7
[2] Chabery M and Viovy J-L 2008 Microfluidic high-throughput encapsulation and hydrodynamic self-sorting of single cells *Proc. Natl Acad. Sci. USA* **105** 3191–6
[3] Yeo T *et al* 2016 Microfluidic enrichment for the single cell analysis of circulating tumor cells *Nat. Sci. Rep.* **6** 22076
[4] Kang D-K, Ali M M, Zhang K, Huang S S, Peterson E, Digman M A, Gratton E and Zhao W 2014 Rapid detection of single bacteria in unprocessed blood using integrated comprehensive droplet digital detection *Nat. Commun.* **5** 5427

[5] Jung W, Han J, Choi J-W and Ahn C H 2015 Point-of-care testing (POCT) diagnostic systems using microfluidic lab-on-a-chip technologies *Microelectron. Eng.* **132** 46–57
[6] Huh D, Leslie D C, Matthews B D, Fraser J P, Jurek S, Hamilton G A, Thorneloe K S, McAlexander M A and Ingber D E 2012 A human disease model of drug toxicity—induced pulmonary edema in a lung-on-a-chip microdevice *Sci. Transl. Med.* **4** 159ra147
[7] Wang X, Phan D T T, Sobrino A, George S C, Hughes C C W and Lee A P 2016 Engineering anastomosis between living capillary networks and endothelial cell-lined microfluidic channels *Lab Chip* **16** 282–90
[8] Langelier S M, Livak-Dahl E, Manzo A J, Johnson B N, Walter N G and Burns M A 2011 Flexible casting of modular self-aligning microfluidic assembly blocks *Lab Chip* **11** 1679–87
[9] Friend J and Yeo L 2010 Fabrication of microfluidic devices using polydimethylsiloxane *Biomicrofluidics* **4** 026502
[10] Hsieh Y-F, Yang A-S, Chen J-W, Liao S-K, Suc T-W, Yeh S-H, Chen P-J and Chen P-H 2014 A Lego®-like swappable fluidic module for bio-chem applications *Sensors Actuators* B **204** 489–96
[11] Yuen P K, Bliss J T, Thompson C C and Peterson R C 2009 Multidimensional modular microfluidic system *Lab Chip* **9** 3303–5
[12] Bhargava K C, Thompson B and Malmstadt N 2014 Discrete elements for 3D microfluidics *Proc. Natl Acad. Sci. USA* **111** 15013–8
[13] Lee K G, Park K J, Seok S, Shin S, Kim D H, Park J Y, Heo Y S, Lee S J and Lee T J 2014 3D printed modules for integrated microfluidic devices *RSC Adv.* **4** 32876–80
[14] Anderson J R, Chiu D T, Jackman R J, Cherniavskaya O, McDonald J C, Wu H, Whitesides S H and Whitesides G M 2000 Fabrication of topologically complex three-dimensional microfluidic systems in PDMS by rapid prototyping *Anal. Chem.* **72** 3158–64
[15] Rhee M and Burns M A 2008 Microfluidic assembly blocks *Lab Chip* **8** 1365–73
[16] Prabowo F, Wing-Keung A L and Shen H H 2015 Effect of curing temperature and cross-linker to pre-polymer ratio on the viscoelastic properties of a PDMS elastomer *Adv. Mater. Res.* **1112** 410–3
[17] Satyanarayana S, Karnik R N and Majumdar A 2005 Stamp-and-stick room-temperature bonding technique for microdevices *J. Microelectromech. Syst.* **14** 392–9